MICROCOPY RESOLUTION TEST CHART

NATIONAL BUREAU OF STANDARDS-1963-A

Office of Naval Research

Contract N00014-78-C-0584

Technical Report No. 6

ULTRASONIC REFLECTION FROM SOLID

HALFSPACES AND FROM SOLID PLATES

by

W. G. Mayer, T. D. K. Ngoc, D. McLennan,

O. J. Leroy and J. M. Claeys

Walter G. Mayer
Principal Investigator
Department of Physics
Georgetown University
Washington, DC 20057

June 1983

JUN 3 0 1983

A

83 06 29 021

SECURITY CLASSIFICATION OF THIS PAGE (When Data Entered)

REPORT DOCUMENTATION PAGE	READ INSTRUCTIONS BEFORE COMPLETING FORM

1. REPORT NUMBER GUUS 06836	2. GOVT ACCESSION NO. AD-A129886	3. RECIPIENT'S CATALOG NUMBER
4. TITLE (and Subtitle) Ultrasonic reflection from solid halfspaces and solid plates		5. TYPE OF REPORT & PERIOD COVERED Technical 1 August 82 - 1 June 83
		6. PERFORMING ORG. REPORT NUMBER TR 6
7. AUTHOR(s) W. G. Mayer, T. D. K. Ngoc, D. McLennan, O.J. Leroy and J. M. Claeys		8. CONTRACT OR GRANT NUMBER(s) N00014-78-C-0584
9. PERFORMING ORGANIZATION NAME AND ADDRESS Physics Department, Georgetown University Washington, DC 20057		10. PROGRAM ELEMENT, PROJECT, TASK AREA & WORK UNIT NUMBERS 121108
11. CONTROLLING OFFICE NAME AND ADDRESS Office of Naval Research, Code 412 Arlington, VA 22217		12. REPORT DATE 17 June 1983
		13. NUMBER OF PAGES 22
14. MONITORING AGENCY NAME & ADDRESS(If different from Controlling Office)		15. SECURITY CLASS. (of this report) Unclassified
		15a. DECLASSIFICATION/DOWNGRADING SCHEDULE

16. DISTRIBUTION STATEMENT (of this Report)

Approved for public release; distribution unlimited

17. DISTRIBUTION STATEMENT (of the abstract entered in Block 20, if different from Report)

Approved for public release; distribution unlimited

18. SUPPLEMENTARY NOTES

19. KEY WORDS (Continue on reverse side if necessary and identify by block number)

ultrasonics, solid halfspace, solid plate, bounded beam,
reflection coefficient

20. ABSTRACT (Continue on reverse side if necessary and identify by block number)

Four aspects of ultrasonic reflectivity are discussed: reflection
coefficient reducibility from thin plate to hlafspace; reflection
of bounded beam; inhomogeneities of reflector; and multifrequency
beam reflection phenomena.

DD FORM 1473 EDITION OF 1 NOV 68 IS OBSOLETE
1 JAN 73
S/N 0102-014-6601 |

This Technical Report consists of reprints of four papers
that deal with four different aspects of the problem of ultra-
sonic reflection from a liquid-solid interface.

The first paper is concerned with the problem of reducing
the mathematical form of the reflection coefficient of an
ultrasonic wave from a solid plate in a liquid to the form of
the reflection coefficient when the solid is considered to be
a halfspace, i.e., from finite to infinite thickness of the
solid layer.

The second paper treats the reflection when the solid is of
finite thickness and a mode of vibration is excited by the in-
cident beam, and when the incident sound signal is a bounded
beam.

The third article describes some effects that may occur if
the solid reflector has small inhomogeneities.

The last paper deals with changes in the reflection effects
when the incident beam contains more than one frequency, as
is often the case when the sound amplitude becomes high.

Walter G. Mayer
Principal Investigator

Washington, DC, June 1983

REDUCIBILITY OF PLANE WAVE REFLECTIVITY FROM A SOLID PLATE IN A LIQUID TO A LIQUID-SOLID INTERFACE.

J.M. Claeys and O.J. Leroy
K.U. Leuven Campus Kortrijk, Kortrijk, Belgium.

T.D.K. Ngoc and W.G. Mayer
Physics Department, Georgetown University, Washington, D.C. 20057, U.S.A.

Abstract

The ultrasonic plane wave reflection coefficient for a flat solid plate immersed in a liquid should be reducible to that for a liquid-solid interface as the plate thickness becomes very large. Existing formulae, which are based on the assumption that propagation vectors are real quantities, do not provide this reducibility. It is shown that reducibility can be achieved only when the propagation vectors are complex quantities, i.e., when absorption is taken into account. The approach given here can thus be used to determine reflectivity for material thicknesses which are neither truly infinite nor very thin. The results provide practical criteria to determine the lower limit of sample thickness that can be considered a half-space.

Introduction

Reflection of ultrasonic plane waves in a liquid-solid-liquid system has been described [1,2] by the amplitude reflection coefficient R_{LSL}, derivable from consideration of the boundary conditions at the interfaces. The plane wave amplitude reflection coefficient R_{LS} for a liquid-solid interface was also obtained [1,2] when the boundary conditions at that interface are taken into account.

It was shown [2] that, beside the material characteristics, the behavior of R_{LSL} is solely determined by one physical parameter, the product frequency f times the thickness d of the solid plate. Mathematical and physical consistency requires that R_{LSL} become R_{LS} as this product tends to infinity. This property has not been established, although it was briefly discussed by Pitts [2]. It is also interesting to understand the behavior of R_{LSL} in this limit as well as to be able to determine the thickness of a solid plate that can be considered a practically acceptable half-space.

Preliminary investigation indicates that absorption plays an essential part when R_{LSL} is examined in the limit: frequency x thickness $\to \infty$. The present paper will study the existence of such a limit with and without absorption being taken into consideration. As a result, reflectivity characteristics of a thick solid plate will also be provided.

1. Plane wave reflection coefficients

The reflection coefficient R_{LSL} for a solid immersed in a liquid, and that for a liquid-solid interface, R_{LS}, are given by [2]

$$R_{LS} = (N_1 + N_2 - N_3) / (N_1 + N_2 + N_3). \qquad (1)$$

$$R_{LSL} = N / (F_a F_s). \qquad (2)$$

where

$$N_1 = (k_s^2 - 2k_x^2)^2. \qquad (3)$$

$$N_2 = 4k_x^2 K_d K_s. \qquad (4)$$

$$N_3 = \rho k_s^4 K_d / K. \qquad (5)$$

$$N = N_1^2 + N_2^2 - N_3^2 + 2N_1 N_2 (1 - \cos P \cos Q) / (\sin P \sin Q). \qquad (6)$$

$$F_a = [(1 - \cos P) / \sin P] \, N_1 + [(1 - \cos Q) / \sin Q] \, N_2 + iN_3. \qquad (7)$$

$$F_s = [(1 + \cos P) / \sin P] \, N_1 + [(1 + \cos Q) / \sin Q] \, N_2 - iN_3. \qquad (8)$$

The symbols used in Eqs. (3-8) are defined as follows:

$$k_x = k \sin\theta_i. \qquad (9)$$

$$\left. \begin{array}{l} k = 2\pi f/v \\[2mm] k_d = 2\pi f/v_d \\[2mm] k_s = 2\pi f/v_s \end{array} \right\} \quad \text{without absorption.} \qquad (10)$$

$$\left. \begin{array}{l} k = (2\pi f/v)(1 + ia/2\pi) \\[2mm] k_d = (2\pi f/v_d)(1 + ia_d/2\pi) \\[2mm] k_s = (2\pi f/v_s)(1 + ia_s/2\pi) \end{array} \right\} \quad \text{with absorption} \qquad (11)$$

$$K = (k^2 - k_x^2)^{1/2}, \quad K_d = (k_d^2 - k_x^2)^{1/2}, \quad K_s = (k_s^2 - k_x^2)^{1/2}. \qquad (12)$$

$$P = dK_d, \quad Q = dK_s, \qquad (13)$$

where

$$\theta_i = \text{angle of incidence},$$

$$\rho = \text{liquid density / solid density},$$

and where v, v_d, v_s and a, a_d, a_s are the measured sound velocities and attenuation per wavelength of the longitudinal waves in the liquid, and the longitudinal and shear waves in the solid, respectively. Consideration of Eqs. (1-13) shows that R_{LSL} depends on fd only through terms involving P and Q. The existence of $\lim_{fd \to \infty} R_{LSL}$ thus dwells essentially on the behaviour of P and Q at such a limit.

II. Limit of R_{LSL} as fd tends to infinity

When absorption is included, that is a, a_d, $a_s \neq 0$, P and Q have the form

$$P = fd(p_R + ip_I) \text{ and } Q = fd(q_R + iq_I).$$

where p_R, p_I, q_R, and q_I, in general are non-zero and finite. The form of the wave functions chosen in the derivation of R_{LSL} implies [2] that p_I and q_I are non-negative, so as to make the sound amplitude decay as physically expected. In the limit of fd tending to infinity, the behaviour of R_{LSL} is governed by terms containing P and Q. It is observed that

$$\cos P = \cos(fdp_R) \cosh(fdp_I) - i\sin(fdp_R) \sinh(fdp_I).$$
$$\sin P = \sin(fdp_R) \cosh(fdp_I) + i\cos(fdp_R) \sinh(fdp_I). \qquad (14)$$

Since p_I is positive

$$\lim_{fd \to \infty} \cosh(fdp_I) = \lim_{fd \to \infty} \sinh(fdp_I) = \lim_{fd \to \infty} \tfrac{1}{2} e^{fdp_I}. \qquad (15)$$

Hence

Hence

$$\lim_{fd \to \infty} \cos P = \lim_{fd \to \infty} \frac{1}{2} e^{fdp_I} \left[\cos(fdp_R) - i\sin(fdp_R) \right],$$

$$\lim_{fd \to \infty} \sin P = \lim_{fd \to \infty} \frac{1}{2} i e^{fdp_I} \left[\cos(fdp_R) - i\sin(fdp_R) \right]. \qquad (16)$$

Equations (14-16) are now used to examine the limit when $fd \to \infty$ of terms involving P and Q in the expression of R_{LSL}. First consider

$$\lim_{fd \to \infty} \frac{1 \pm \cos P}{\sin P} = \lim_{fd \to \infty} \frac{1 \pm \frac{1}{2} e^{fdp_I} \left[\cos(fdp_R) - i\sin(fdp_R) \right]}{\frac{1}{2} i e^{fdp_I} \left[\cos(fdp_R) - i\sin(fdp_R) \right]}. \qquad (17)$$

but

$$\lim_{fd \to \infty} \left[1 + \frac{1}{2} e^{fdp_I} \cos(fdp_R) \right] = \lim_{fd \to \infty} \left\{ e^{fdp_I} \left[e^{-fdp_I} \pm \frac{1}{2} \cos(fdp_R) \right] \right\}.$$

$$= \qquad = \lim_{fd \to \infty} \left[\pm \frac{1}{2} e^{fdp_I} \cos(fdp_R) \right]. \qquad (18)$$

since p_I is always positive, as mentioned earlier.

Hence

$$\lim_{fd \to \infty} \frac{(1 \pm \cos P)}{\sin P} = \lim_{fd \to \infty} \frac{\pm \frac{1}{2} e^{fdp_I} \left[\cos(fdp_R) - i\sin(fdp_R) \right]}{\frac{1}{2} i e^{fdp_I} \left[\cos(fdp_R) - i\sin(fdp_R) \right]}. \qquad (19)$$

or

$$\lim_{fd \to \infty} \frac{(1 \pm \cos P)}{\sin P} = \mp i. \qquad (20)$$

Similarly, it can be shown that

$$\lim_{fd \to \infty} \frac{(1 \pm \cos Q)}{\sin Q} = \mp i. \qquad (21)$$

Next consider the same limit of the remaining term involving P and Q,

$$\lim_{fd \to \infty} \frac{1 - \cos P \cos Q}{\sin P \sin Q}$$

In view of Eq. (16), the real part of $(1 - \cos P \cos Q)$ is seen to behave as

$$\lim_{fd \to \infty} \mathrm{Re}(1 - \cos P \cos Q) =$$

$$\lim_{fd \to \infty} \left\{ 1 - \frac{1}{4} e^{fd(p_I + q_I)} \left[\cos(fdp_R) \cos(fdq_R) - \sin(fdp_R) \sin(fdq_R) \right] \right\},$$

$$= \lim_{fd \to \infty} \left\{ - \frac{1}{4} e^{fd(p_I + q_I)} \left[\cos(fdp_R) \cos(fdq_R) - \sin(fdp_R) \sin(fdq_R) \right] \right\}, \qquad (22)$$

where a manipulation similar to that of Eq. (18) has been performed.

Use of Eq. (22) yields

$$\lim_{fd \to \infty} \frac{1 - \cos P \cos Q}{\sin P \sin Q}$$

$$= \lim_{fd \to \infty} \frac{-\frac{1}{4} e^{fd(p_I + q_I)} (\cos fdp_R - i\sin fdp_R)(\cos fdq_R - i\sin fdq_R)}{\frac{1}{4} i^2 e^{fd(p_I + q_I)} (\cos fdp_R - i\sin fdp_R)(\cos fdq_R - i\sin fdq_R)}, \qquad (23)$$

or

$$\lim_{fd \to \infty} \frac{1 - \cos P \cos Q}{\sin P \sin Q} = 1. \qquad (24)$$

Substitution of Eqs. (20), (21) and (24) into Eq (2) results in

$$\lim_{fd \to \infty} R_{LSL} = \frac{N_1^2 + N_2^2 - N_3^2 + 2N_1 N_2}{(iN_1 + iN_2 + iN_3)(-iN_1 - iN_2 - iN_3)} \quad . \tag{25}$$

$$= \frac{(N_1 + N_2)^2 - N_3^2}{(N_1 + N_2 + N_3)^2} = \frac{N_1 + N_2 - N_3}{N_1 + N_2 + N_3} \quad . \tag{26}$$

or

$$\lim_{fd \to \infty} R_{LSL} = \lim_{fd \to \infty} R_{LS}. \tag{27}$$

III. Discussion

The above derivation establishes that the plane wave reflectivity from a solid plate immersed in a liquid will become that from a liquid-solid interface when the plate thickness, normalized with respect to the acoustic wavelength, tends to infinity. This result holds only when absorption in the media is taken into account. Without absorption being considered, such limit does not exist. In particular, when absorption is neglected it can be shown that R_{LSL} tends to R_{LS} only when the incident angle is larger than the shear critical angle. This is graphically illustrated in Figure 1, where the modulus of R_{LSL} is plotted against the incident angle with a very high value of fd, 50km/s, for a water-brass-water system. There the $|R_{LSL}|$ curve is seen to be irreducible to the $|R_{LS}|$ one when absorption is neglected. It is worth noting that near the Rayleigh critical angle R_{LSL} always tends to R_{LS} no matter whether absorption is considered or not. This confirms the understanding that Rayleigh surface waves or Rayleigh-type Lamb waves are always physically confined to the first interface, which is the one on which the incoming sound waves are incident. The physical location of the second interface obviously does not affect the behaviour of these propagation modes.
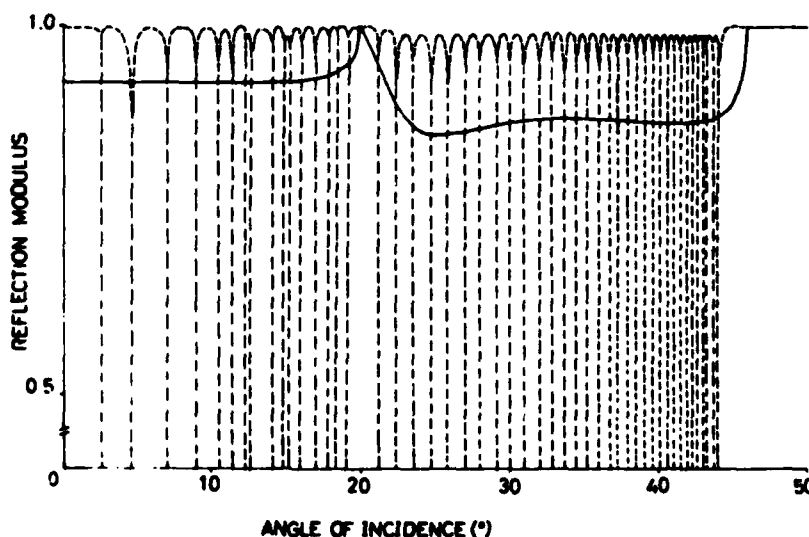

Figure 1. Reflection amplitude for a lossless water-brass-water system with fd = 50km/s. The solid curve is reflection amplitude for a lossless water-brass system.
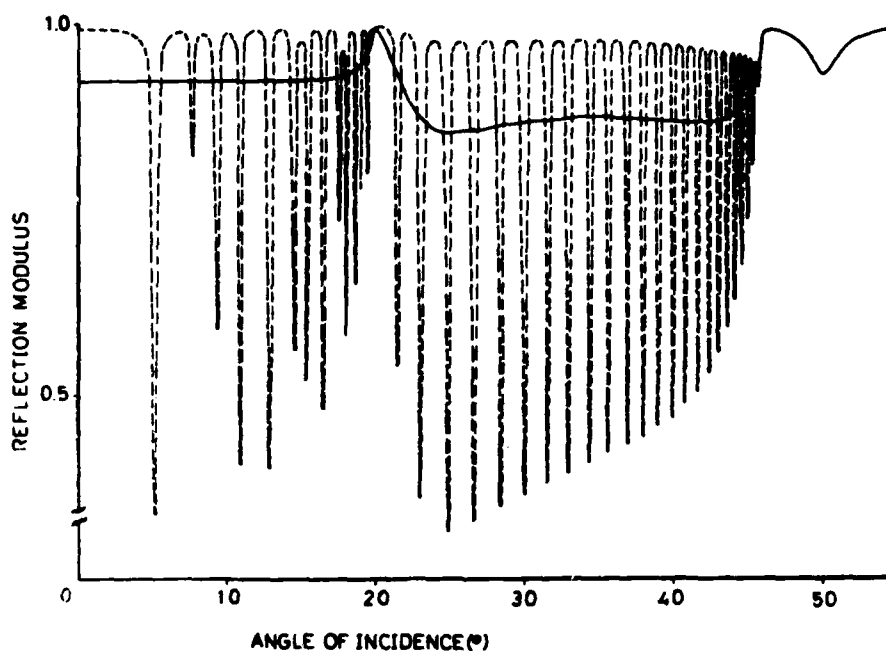
Figure 2. Reflection amplitude for an absorptive water-brass-water system with fd = 31.75km/s and f = 5MHz. The reflection amplitude for a water-brass interface with absorption for the same frequency is illustrated by the solid curve.

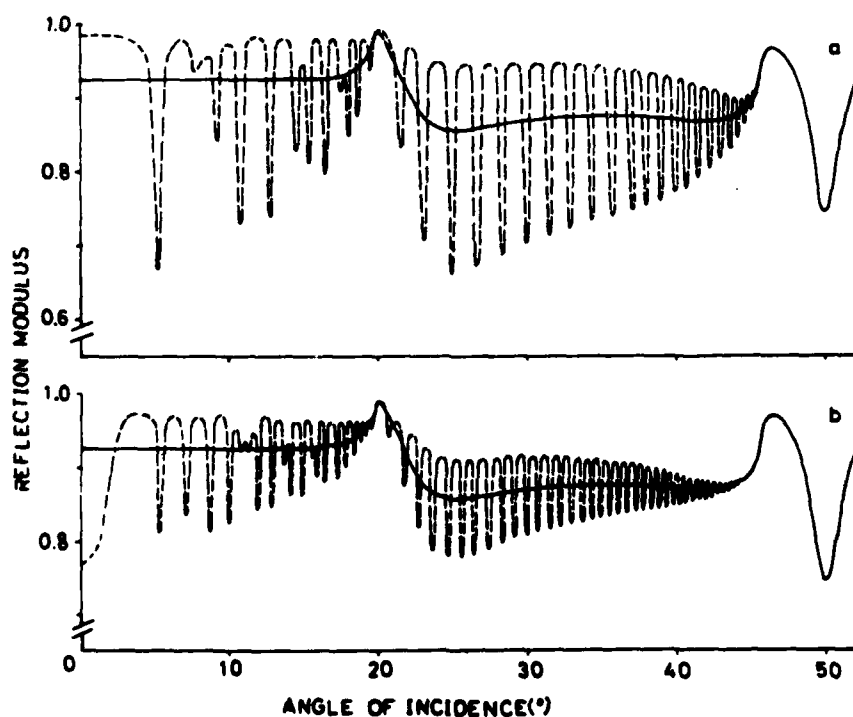Figure 3. Reflection amplitude for an absorptive water-brass-water system with f = 10MHz and (a) fd = 31.75km/s and (b) fd = 63.5km/s, respectively. The reflection amplitude for absorptive water-brass systems of the same frequency is plotted in the solid curve.

Figures 2 and 3 demonstrate graphically the behaviour of $|R_{LSL}|$ when absorption is included for a water-brass-water system. Attenuation data used for brass are derived from measurements made by Papadakis [3] and those for water provided by Pinkerton [4]. The modulus of R_{LSL} is presented in Figure 2 for $f = 5MHz$, $fd = 31.75km/s$, and in Figure 3 for $f = 10MHz$, $fd = 31.75$ and $63.5km/s$. Comparison of the three curves of Figures 2 and 3 leads to the following observations: (i) as fd becomes larger $|R_{LSL}|$ behaves more like $|R_{LS}|$; and (ii) for the same fd value $|R_{LSL}|$ tends to $|R_{LS}|$ faster for higher absorption.
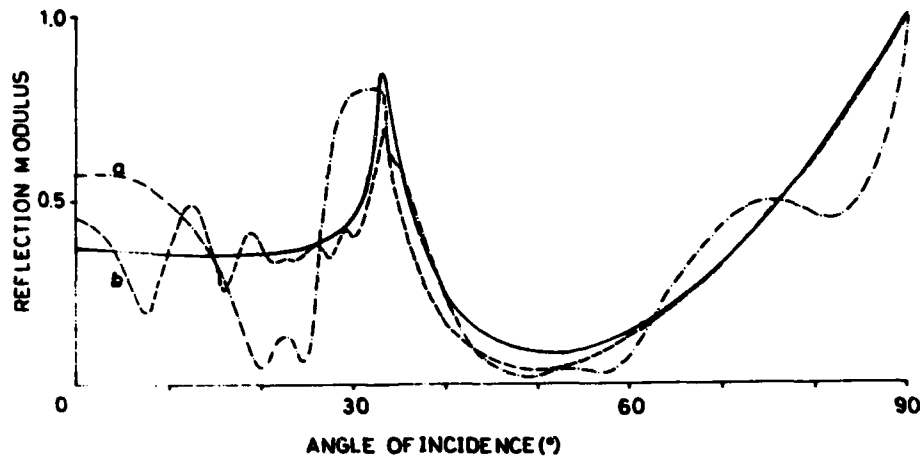

Figure 4. Reflection amplitude for an absorptive water-Plexiglas-water system with (a) $fd = 3.18km/s$, $f = 2MHz$ and (b) $fd = 12.7km/s$, $f = 4MHz$. The reflection amplitude for an absorptive water-Plexiglas interface at $2MHz$ is described by the solid curve.
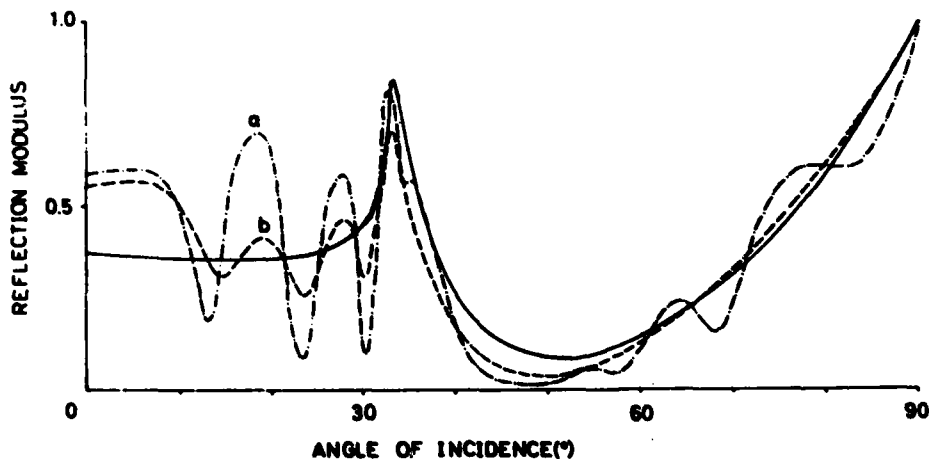
Figure 5. Reflection amplitude for an absorptive water-Plexiglas-water system with $fd = 6.35km/s$ but (a) $f = 2MHz$ and (b) $f = 4MHz$. The reflection amplitude for an absorptive water-Plexiglas interface is described by the solid curve.

Since the physical properties of Plexiglas are remarkably different from brass, it is interesting to see how $|R_{LSL}|$ behaves in comparison with $|R_{LS}|$ for a water-Plexiglas-water system. Similar results are obtained in this case except for the fact that with a highly absorptive substance such as Plexiglas R_{LSL} reduces to R_{LS} at much lower values of fd. These are illustrated in Figures 4 and 5. The attenuation data used for Plexiglas are taken from Ngoc [5]. The same observations as made for water-brass-water also apply here: $|R_{LSL}|$ approaches $|R_{LS}|$ faster for higher fd values and absorption.

IV. Conclusion

The above results provide a unified picture of plane wave reflectivity for liquid-solid and liquid-solid-liquid layered systems. It is seen that absorption plays an essential role in verifying that R_{LSL} is reducible to R_{LS} when the thickness of the solid plate becomes very large compared to the acoustic wavelength. The question of how thick a solid plate can be considered to be a half-space for practical purposes must be addressed with proper consideration of the absorption characteristics of the media involved.

References

[1]   Brekhovskikh, L.M., *Waves in Layered Media*, Academic Press, New York, 1960.

[2]   Pitts, L.E., *A Unified Theoretical Description of Ultrasonic Beam Reflections for a Solid Plate in a Liquid*, Ph.D. Thesis, Physics Department, Georgetown University, Washington, D.C. 1975.

[3]   Papadakis, E.P., *J. Acoust. Soc. Am.*, **37**, 711, 1965.

[4]   Pinkerton, J.M.M., *Nature*, **160**, 128, 1947.

[5]   Ngoc, T.D.K., *Influence of Absorption on Ultrasonic Nonspecular Reflectivity*, Ph.D. Thesis, Physics Department, Georgetown University, Washington, D.C., 1979.

(Received 19 October 1981)

Correspondence

Influence of Plate Mode Structure and Gaussian Beam Profile Characteristics on Ultrasonic Reflection and Transmission

TRAN D. K. NGOC AND WALTER G. MAYER

Abstract—It is shown why ultrasonic beam reflection from, and transmission through, a solid plate immersed in a liquid may be non-specular, depending on beamwidth and the structure of the normal modes of vibration of the plate. The analysis is carried out for Gaussian incident beams.

INTRODUCTION

The profile of an acoustic beam reflected from or transmitted through a layered medium has recently been calculated by several authors. An analytical method was used by Bertoni and Tamir [1] for a liquid–solid interface and by Pitts [2] and Ng [3] for a solid plate immersed in a liquid, respectively. Ngoc and Mayer [4]–[6] determined these profiles numerically and showed that the use of a numerical integration method eliminated some of the limitations encountered in the analytical formulation.

For a solid plate immersed in a liquid, Ngoc and Mayer [6] investigated the general features of the reflected and transmitted beam profiles for incidence at plate-mode and between-mode angles. Plate-mode angles of incidence are defined as the incident angles of the impinging plane waves at which leaky Lamb waves are generated, while the latter type of incidence denotes an angle of incidence located exactly between two adjacent plate-mode angles. Changes in profiles were also studied as a function of angle of incidence and beamwidth. However, there are neither systematic studies of profile changes nor of the relationship between the mode structure of a loaded solid plate and the beam structure of a Gaussian beam.

This correspondence is concerned with profile changes in a broader perspective in order to provide better practical insight into nonspecular reflection and transmission phenomena. A nonspecularly reflected or transmitted beam will be viewed as a result of the interplay between plate-mode structure and beam characteristics. Emphasis will therefore be placed on using an adequate range of values for beamwidth as well as a more representative mode structure.

MATHEMATICAL AND PHYSICAL DESCRIPTION

The sound field of a bounded beam reflected from or transmitted through a solid plate immersed in a liquid is represented [6] by

$$U^{(R)}(x, 0) = (2\pi)^{-1} \int_{k_i - \pi/W_0}^{k_i + \pi/W_0} R(k_x) V(k_x) \cdot \exp(ik_x x)\, dk_x, \tag{1}$$

$$U^{(T)}(x, -d) = (2\pi)^{-1} \int_{k_i - \pi/W_0}^{k_i + \pi/W_0} T(k_x) V(k_x) \cdot \exp[i(k_x x - k_z d)]\, dk_x, \tag{2}$$

where $U^{(R)}$ and $U^{(T)}$ are the sound amplitudes of the reflected and transmitted fields, and $R(k_x)$ and $T(k_x)$ are the plane wave reflection and transmission coefficients. The x-direction is given by the propagation direction of the Lamb wave, and the thickness of the plate, d, is measured along the z-direction. The other symbols used in above expressions are defined as follows:

k_x x-component of the wave vector k,
k_z $= (k^2 - k_x^2)^{1/2}$,
$V(k_x)$ Fourier transform of incident beam, defined in (4),
k_i $= (\omega/v) \sin \theta_i$,
ω sound angular frequency,
θ_i incident angle,
v sound speed in the liquid,
W_0 $= W/\cos \theta_i$,
W half-width of the Gaussian beam.

Equations (1) and (2) are based on the fact that an incident beam can be represented by a superposition of a finite number of plane waves of different incident angle. The reflected and transmitted beams are then constructed from the constituent plane waves after they have interacted with the layered system via the reflection or transmission coefficient, derived from the plane wave theory. In general, the resulting reflected or transmitted beam profiles are determined by the physical characteristics of the incident beam and the layered medium, which here is taken to be a solid plate immersed in a liquid.

A. Beam Characteristics

A Gaussian beam of width $2W$ incident at an angle θ_i is characterized at $z = 0$, the boundary between the liquid and the solid plate, by

$$U_{\text{inc}}(x, 0) = \exp[-(x/W_0)^2 + ixk_i], \tag{3}$$

whose Fourier transform in the k_x domain is

$$V(k_x) = \pi^{1/2} W_0 \exp[-(k_x - k_i)^2 (W_0/2)^2]. \tag{4}$$

Equation (3) implies that the incident angles of constituent incoming plane waves are perturbed about θ_i and that this angular spreading is a function of the beamwidth. For a given sound frequency, this angular spreading can be measured in terms of θ_{HW}, an angle in degrees, expressing the half-width of the Gaussian function $V(k_x)$, and θ_{HW} can be written [6] as

$$\theta_{\text{HW}} = \sin^{-1}(\sin\theta_i + 0.53\, W_k) - \sin^{-1}(\sin\theta_i - 0.53\, W_k), \tag{5}$$

where $W_k = (\pi v \cos \theta_i)/(\omega W)$.
Some simple manipulation of (5) gives rise to

$$\theta_{\text{HW}} \simeq 30.4 \lambda/W, \tag{6}$$

where λ is the sound wavelength in the liquid. The identity (6) is a good approximation when λ/W is less than unity. Typical values of θ_{HW} are summarized in Table I for a frequency of 2 MHz and for several values of W under consideration.

B. Mode Structure

The transmission or reflection coefficient for a solid plate immersed in a liquid can be used to describe the acoustical characteristics of the plate. In general, these coefficients are functions of the product fd (frequency times plate thickness).

TABLE I

ANGULAR SPREADING OF A GAUSSIAN INCIDENT BEAM FOR
VARIOUS BEAMWIDTH AND FREQUENCY OF 2 MHz

W (in)	λ/W	θ_{HW} (degrees)
$\frac{1}{8}$	0.2362	14.4
$\frac{1}{4}$	0.1181	7.2
$\frac{1}{2}$	0.0591	3.6
$\frac{3}{4}$	0.0394	2.4
2	0.0147	0.89
8	0.0037	0.22
32	0.0009	0.06

TABLE II

MODE STRUCTURE OF A WATER–BRASS–WATER SYSTEM FOR
$fd = 7$ MHz · mm

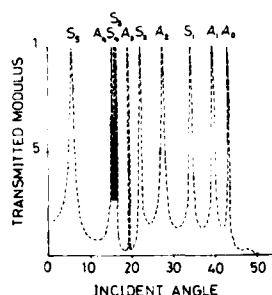| Modes	θ_p (degrees)	$S(p_n, p_m)$
$A_0(S_0)$	43.2	
A_1	39.6	3.6
S_1	34.2	5.4
A_2	27.4	6.8
S_2	22.05	5.35
A_3	19.3	2.75
S_3	16.25	3.05
S_4	16.0	0.25
A_4	15.25	0.75
S_5	5.65	9.6

Fig. 1. Plane wave transmission modulus for water–brass–water system with fd = 7.0 MHz · mm. Standard plate-mode nomenclature is used to identify plate-mode angles of incidence.

Their analytical behavior is completely determined by a number of pole-zero pairs [6]. These pole-zero pairs are associated with plate-mode angles of incidence. The complete set of plate modes forms the mode structure of the layered system under consideration. Thus the mode structure identifies the plate-mode angles θ_p and the angular separation between them. In the following, $S(p_n, p_m)$ denotes the angular separation between modes p_n and p_m. Table II describes the mode structure of a brass plate immersed in water for an fd of 7 MHz · mm. This value of fd was chosen so that $S(p_n, p_m)$ has a wide range of values, which are also comparable to the values of θ_{HW} listed in Table I. The corresponding transmission coefficient is shown in Fig. 1. In both Table II and Fig. 1, the letters A and S denote symmetric and antisymmetric modes, respectively.

CALCULATED RESULTS

The expressions given above can be used to calculate the energy or amplitude profiles of reflected or transmitted sound fields produced by an incident Gaussian beam. It is well-
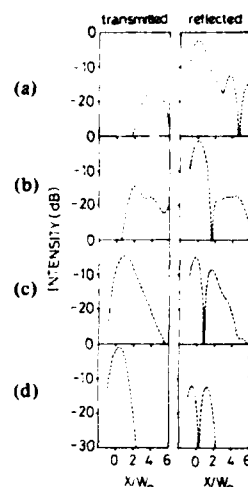

Fig. 2. Transmitted and reflected beam profiles for water–brass–water, 7 MHz · mm and plate-mode incidence at 39.6°. Beamwidth values are (a) $\frac{1}{8}$ in, (b) $\frac{1}{4}$ in, (c) 2 in, and (d) 8 in.

known that the reflected or transmitted sound field quite frequently is no longer Gaussian, that the reflected beam often is "displaced" [7], sometimes split into distinct beams with an energy-null separating the sections [8], or sometimes reflected as a Gaussian beam without any apparent change from the original Gaussian profile.

These nonspecular reflection and transmission phenomena can be predicted if one takes into account the mode structure of the plate, the width and frequency of the incident beam, and the angle of incidence as given in (1)–(6).

As an example of such calculations, consider a brass plate immersed in water, with the parameter fd being 7 MHz · mm and the Gaussian incident beam having a frequency $f = 2$ MHz. Two series of calculations are discussed here for two types of incidence: incidence at the plate-mode angle $\theta_i = 39.6°$ and incidence at the between-mode angle $\theta_i = 41.4°$.

For the selected A_1 plate-mode incidence angle, four profiles are calculated for the following beamwidths: (a) $\frac{1}{8}$ in, (b) $\frac{1}{4}$ in, (c) 2 in, and (d) 8 in. The resulting profiles are plotted in Fig. 2.

(a) Since $\frac{1}{8}$ in is a rather narrow beamwidth, the angular spreading θ_{HW} covers three adjacent modes, A_0 on the left and S_1 and A_2 on the right. With this wide coverage of θ_{HW}, the reflected profile shows a complicated pattern with more than one secondary peaks and intensity nulls, caused by the influence of the involved neighboring modes. The transmitted beam exhibits a lateral displacement of approximately $2W_0$, which is the projection of the beamwidth onto the reflecting interface.

(b) A beamwidth of $\frac{1}{4}$ in implies that the angular spreading θ_{HW} is 7.2°, including on both sides two modes, A_0 and S_1. The reflected profile exhibits only one intensity null and the only secondary peak, broadened considerably, indicates competing influences of the adjacent modes. In the transmitted profile, this phenomenon also appears in the trailing edge of the sound field, while the lateral displacement is decreased but still significant, extending to approximately W_0.

(c) For a beamwidth of 2 in, the angular spreading $\theta_{HW} = 0.89°$ is narrowly centered about the A_1 mode. Both reflected and transmitted profiles are influenced only by this mode. These profiles are typical whenever only one mode is involved.

(d) With a very large beamwidth, 8 in in this case, the angular spreading becomes extremely small such that the beam profiles are strongly determined by the behavior of the plane wave coefficients. Almost total transmission is obtained with no nonspecular features present. The reflected profile, although of very low intensity, retains its nonspecular features
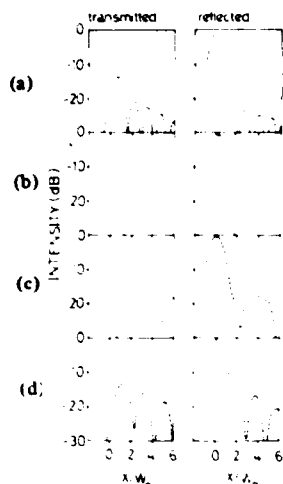
Fig. 3. Transmitted and reflected beam profiles for water–brass–water.
7 MHz · mm and between-mode incidence at 41.4°. Beamwidth value
values are (a) $\frac{3}{4}$ in, (b) 2 in, (c) $\frac{1}{4}$ in, and (d) $\frac{1}{2}$ in.

because of an extremely sharp phase shift of the reflection coefficient at plate-mode incidence.

The results of calculations for the between-mode angle of incidence are shown in Fig. 3 for beamwidths of (a) $\frac{3}{4}$ in, (b) 2 in, (c) $\frac{1}{4}$ in, and (d) $\frac{1}{2}$ in. The following features should be noted.

(a) The beamwidth of $\frac{3}{4}$ in was chosen as the first calculation value for a specific reason. Special nonspecular features, consisting of a series of closely spaced secondary peaks, were observed to be most pronounced for this beamwidth in both reflected and transmitted profiles. In this case $\theta_{HW} = 2.4°$, which is of the right magnitude to induce competing influences of modes A_0 and A_1.

(b) When the beamwidth is much larger, 2 in, then $\theta_{HW} = 0.89°$. This is small enough to eliminate essentially the influence of any mode; thus nonspecular phenomena disappear and both the high reflection and low transmission are entirely specular.

(c) For a beamwidth of $\frac{1}{4}$ in, the angular spreading becomes rather large, with $\theta_{HW} = 7.2°$. This includes only the modes A_0 and A_1, and the resulting transmitted and reflected profiles indicate that a combination of two modes behaves like a single mode if the value of θ_{HW} of the incoming beam is much larger than the mode spacing.

(d) With the beamwidth being $\frac{1}{2}$ in and an associated θ_{HW} of 3.6°, the resulting profiles are a mixture of those described in (a) and (c) above, manifesting both interference and single-mode nonspecular features in the reflected and transmitted profiles.

CONCLUSION

It has been demonstrated that the basic features of non-specularly reflected and transmitted beam profiles for a solid plate immersed in a liquid can be predicted from comparison of the incident beamwidth, i.e., its angular spreading of its Fourier transform and the mode structure in the neighborhood

of the incident angle. The observations can be summarized as follows.

1) Plate-Mode Incidence: For a rather wide Gaussian beam, i.e., very small angular spreading, nonspecular features are not significant, and beam profiles are determined essentially by plane wave reflection coefficients. When the angular spreading covers several modes, i.e., for narrow beams, the beam profiles become nonspecular and complex, indicating the competing influence of these modes. Typical single-mode profiles are obtained when the angular spreading of the beam is significant and includes only one mode.

2) Between-Mode Incidence: Special nonspecular phenomena are observable when $\theta_{HW} \simeq S(p_n, p_m)/2$. When the angular spreading is very small, reflected and transmitted beam profiles are specular. For a very large angular spreading, the influence of two modes is essentially the same as that of a single mode, and the resulting beam profiles are similar to single mode profiles.

The analysis presented here can also be used to explain the results of Firestone [9], who was unable to produce total transmission through plates at all the angles of incidence where a plate mode should have been generated; neither $S(n_p, p_m)$ nor θ_{HW} were considered in his experiments.

In view of the approach outlined above, one can also explain why Schoch [7] was unable to identify experimentally all possible modes of a plate of a given fd. His criterion for the excitation of a mode was the observation of "lateral beam displacement"; however, such a displacement occurs only when the beamwidth and the mode spacing have a very specific relationship to each other. Using Schoch's criterion, modes other than those identified by him can be observed simply by adjusting the beamwidth in relation to the known mode spacing.

Finally, applying the present analysis to the known mode spacing where fd becomes very large (the typical liquid–solid single boundary) one can see why only one of the extremely large number of possible modes, the Rayleigh mode, will yield nonspecular reflection. As fd becomes very large, all the possible Lamb modes are extremely closely spaced and only the lowest mode, the Rayleigh mode, is angularly separated from the rest. Thus even a rather wide incident beam has a value of θ_{HW}, which although it may well be much less than 1°, is much larger than the $S(p_n, p_m)$ for the Lamb modes, and as was pointed out above, this situation will result in simple specular reflection. Only the separated Rayleigh mode is able to produce nonspecular reflectivity effects, provided the incident beam has the correct angular spreading.

REFERENCES

[1] H. L. Bertoni and T. Tamir, *J. Appl. Phys.*, vol. 2, p. 157, 1973.
[2] L. F. Pitts, "A unified theoretical description of ultrasonic beam reflections from a solid plate in a liquid," Ph.D. Thesis, Physics Department, Georgetown University, Washington, DC, 1975.
[3] K. W. Ng, "Nonspecular ultrasonic bounded beam transmission through solid plates," Ph.D. Thesis, Physics Department, Georgetown University, Washington, DC, 1979.
[4] T.D.K. Ngoc and W. G. Mayer, *J. Appl. Phys.*, vol. 50, p. 7948, 1979.
[5] —, *J. Acoust. Soc. Am.*, vol. 67, p. 1149, 1980.
[6] —, *IEEE Trans. Son. Ultrason.*, vol. SU-27, p. 229, 1980.
[7] A. Schoch, *Acustica*, vol. 2, p. 18, 1952.
[8] W. G. Neubauer, *J. Appl. Phys.*, vol. 44, p. 48, 1973.
[9] F. A. Firestone, *Non-Destructive Testing*, vol. 7, p. 2, 1948.

Characterization of Localized Surface Elastic Defects by Nonspecular Reflection at the Rayleigh Angle

Tran D. K. Ngoc[1] and Walter G. Mayer[1]

The relationships between characteristics of elastic defects and nonspecular features of bounded ultrasonic beams reflected at the Rayleigh angle from a liquid-solid interface are investigated. The results can serve as a theoretical basis for interpretation of Rayleigh angle nonspecularly reflected beam profiles as characterization of localized surface elastic defects.

1. INTRODUCTION

When an ultrasonic bounded beam is incident at a liquid-solid interface, the reflected beam very often has a lower intensity level but the same intensity distribution profile. However, at Rayleigh-angle incidence, the reflected intensity profile is known to display a number of distinct features that substantially deviate from the profile of the incident beam. These features, which are normally referred to as nonspecular reflection effects, may include a lateral beam displacement, one or more minimum intensity areas, and a trailing sound field. Such a nonspecularly reflected profile is illustrated in Fig. 1.

Several authors,[1,2] although using different mathematical techniques, were able to describe nonspecular reflectivity at the critical Rayleigh angle for a liquid-solid interface. Nonspecular reflectivity was also demonstrated and described[3] for incidence near the longitudinal critical angle. Study of nonspecular effects was then extended to a more complex structure, that of a solid plate immersed in a liquid, in which both reflected and transmitted beams were
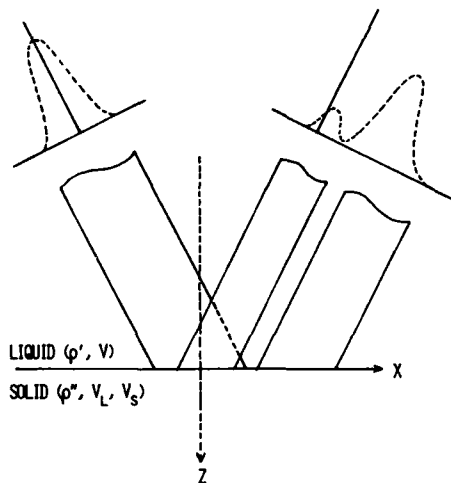
Fig. 1. Coordinate system and a typical nonspecularly reflected beam profile at the Rayleigh angle.

shown[4,5] to possess nonspecular features at critical Lamb mode angles.

It was realized that the distinct features associated with nonspecular reflection could be used to characterize the elastic properties, or any derivation therefrom, of solid materials. These features can constitute a readily recognizable signature that is uniquely

[1] Physics Department, Georgetown University, Washington, D.C. 20057.

related to small variations of certain elastic properties of the medium to be examined. Mayer and Ngoc[6,7] have demonstrated the utility of nonspecular features as a signature to detect local fluctuations of elastic properties. Their experimental results (see Fig. 2) and preliminary calculations showed that the profile of a 2 MHz beam reflected from a water-brass interface underwent a substantial shift in intensity between two sections of a beam as the beam was scanned across the known location of an elastic defect. Chimenti and Adler[8] have used Rayleigh-angle incidence for the detection of small surface-connected fatigue cracks in a titanium alloy, demonstrating that the presence of a fatigue crack leads to a reduction in intensity over one section of the nonspecularly reflected beam.

This paper is a theoretical investigation of the relationships between characteristics of elastic defects and nonspecular features of a bounded beam re-

Fig. 2. Schlieren photographs showing profile changes due to an elastic defect for a 2 MHz beam incident onto a water-brass interface at the Rayleigh angle. (a) no defect; (b) with defect. (After ref. 6.)

flected from a liquid-solid interface at the Rayleigh angle. It is then intended to serve as a theoretical basis for interpretation of Rayleigh-angle nonspecularly reflected profiles, when they are used as a signature to characterize a localized surface elastic defect.

2. NONSPECULAR REFLECTION AT RAYLEIGH ANGLE

Mathematically, a bounded ultrasonic beam can be described as a superposition of an infinite number of plane waves of different amplitude which have the same frequency but are incident at slightly different angles centered about the principal incident direction. In Fig. 1, an ultrasonic beam bounded in the (x, z) plane and uniform in the y dimension is shown to be incident at an angle θ_i, which is assumed to be the principal incident direction. The beam is characterized by angular frequency $\omega = 2\pi f$ and contained within an effective width of $2w$, which is projected onto the interface along the x axis as $2w_0$.

It was shown through Fourier analysis[8] that the sound field of an incident beam can be uniquely determined at any point in the (x, z) plane if its field distribution is given in any plane. Consequently, once the sound field is determined in the plane $z = 0$, a well-defined incident beam can be specified anywhere by the following Fourier integral transform pair:

$$U_{\text{inc}}(x, z) = (2\pi)^{-1} \int_{k_i - \pi/w_0}^{k_i + \pi/w_0} V(k_x)$$

$$\cdot \exp\left[i(xk_x + zk_z)\right] dk_x \qquad (1)$$

$$V(k_x) = \int_{-w_0}^{w_0} U_{\text{inc}}(x, 0)\exp(-ixk_x)\, dx \qquad (2)$$

In (1) and (2), k is the wave vector variable whose x and z components are k_x and k_z; the wave vector $k_i = (\omega/v) \sin\theta_i$ describes the central direction of propagation of the incident beam; $V(k_x)$ is the amplitude of the constituent plane waves; $U_{\text{inc}}(x, 0)$ is the field distribution of the incident beam in the plane $z = 0$; and the time-dependent factor, $\exp(-i\omega t)$, is suppressed for convenience. In all calculations described in this paper, the incident beam is assumed to have a Gaussian distribution, which is characterized at the plane $z = 0$ by

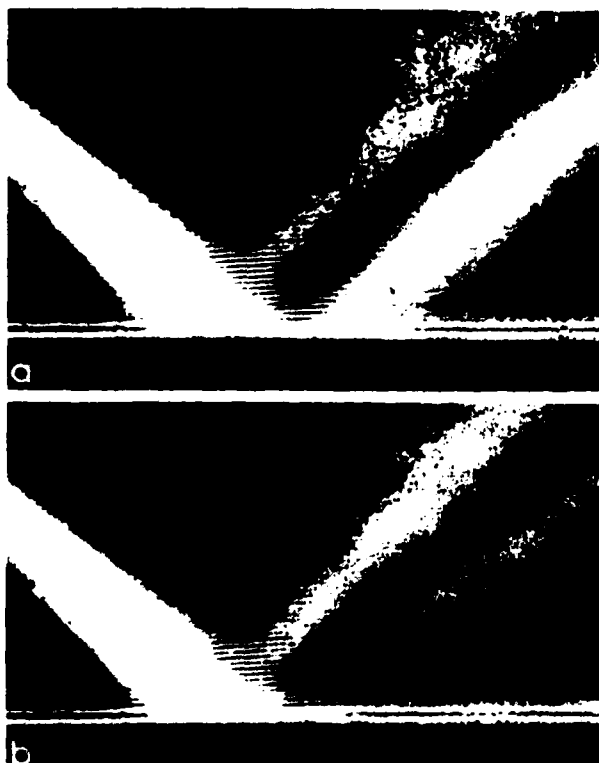$$U_{\text{inc}}(x, 0) = \exp\left[-(x/w_0)^2 + ixk_x\right] \qquad (3)$$

Hence, from (2), the specific form of $V(k_x)$ is

$$V(k_x) = \pi^{1/2} w_0 \exp\left[-(k_x - k_i)^2 (w_0/2)^2\right] \quad (4)$$

The mathematical representation that describes the incident beam by (1) can be extended to represent a bounded ultrasonic beam reflected from a liquid-solid interface. In the same manner, the reflected beam is a superposition of constituent plane waves, which are individually reflected according to the plane wave reflection coefficient $R(k_x)$ associated with the liquid-solid structure. In other words, the sound field of the reflected beam can be represented by

$$U(x, z) = (2\pi)^{-1} \int_{k_i - \pi/w_0}^{k_i + \pi/w_0} R(k_x) V(k_x)$$

$$\cdot \exp\left[i(xk_x + zk_z)\right] dk_x \quad (5)$$

where $R(k_x)$ is given[2] by

$$R(k_x) = \frac{\left(k_s^2 - 2k_x^2\right)^2 + 4k_x^2 K_s K_d - \rho k_s^4 K_d/K}{\left(k_s^2 - 2k_x^2\right)^2 + 4k_x^2 K_s K_d + \rho k_s^4 K_d/K} \quad (6)$$

in which

$$\rho = \rho'/\rho''$$

$$k = (\omega/v)(1 + ia/2\pi)$$

$$k_d = (\omega/v_d)(1 + ia_d/2\pi)$$

$$k_s = (\omega/v_s)(1 + ia_s/2\pi)$$

$$K = \left(k^2 - k_x^2\right)^{1/2}$$

$$K_d = \left(k_d^2 - k_x^2\right)^{1/2}$$

$$K_s = \left(k_s^2 - k_x^2\right)^{1/2} \quad (7)$$

The quantities a, a_d, and a_s in (7) denote attenuation per wavelength for sound waves in liquid and for longitudinal and shear waves in solid, respectively. The integral in (5) can be carried out to provide the distribution profile of the sound field of the reflected beam for any incident angle. For example, the intensity profile of a 2 MHz, 20 mm Gaussian beam reflected from a water-stainless steel interface at the Rayleigh angle is presented in Fig. 3, where the profile (solid curve) is seen to have primarily two sections, with the higher one being laterally displaced to the right and the lower one to the left of the center
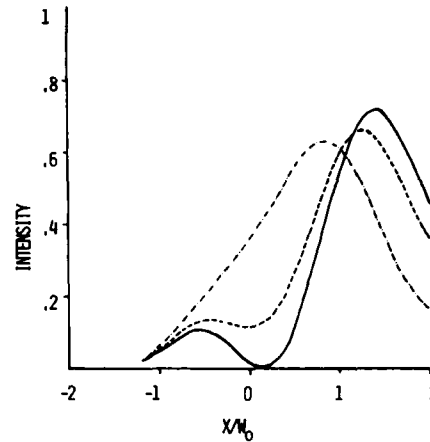

Fig. 3. Variations of reflected profile as v_S is changed with v_L and density is kept constant. ($\rho'' = 7.94$, $v_L = 5.84$ km/s, and $\theta_i = \theta_R$ corresponding to $v_S = 3.13$ km/s).

of the beam. This is a typical nonspecularly reflected profile having two sections separated by an intensity minimum and a trailing field away from the insonified area.

3. APPLICATION OF RAYLEIGH-ANGLE NONSPECULAR REFLECTIVITY TO DEFECT CHARACTERIZATION

The very distinct features produced by the nonspecular effects present themselves as an effective means to characterize elastic properties associated with the material medium under investigation, provided small fluctuations in the elastic properties can be related to discernible changes in the nonspecular features of the reflected profile. In order to determine whether these changes are discernible, or if any exist at all, reflected profiles were calculated for Rayleigh-angle incidence as the key elastic properties of stainless steel were varied. Starting with the initial selection of elastic parameters, $\rho = 7.94$, $v_L = 5.84$ km/s, and $v_S = 3.13$ km/s, each of these parameters was varied while keeping the others fixed. It was found that the nonspecular features were quite insensitive to variation of ρ and v_L. However, even small fluctuations in v_S resulted in substantial changes in the nonspecularly reflected profile.

Figure 3 shows the results of calculations where the value of the shear wave velocity was changed from the assumed value of $v_S = 3.13$ km/s to 3.09 and 3.05 km/s, respectively. It is seen that a change
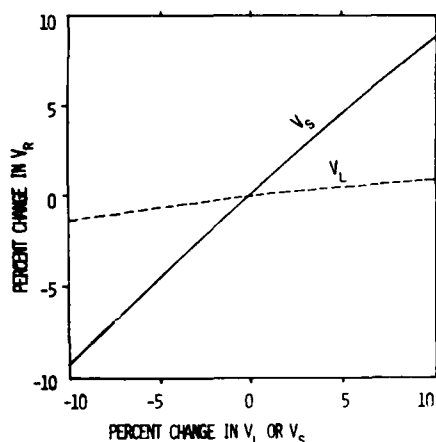
Fig. 4. Percentage change in v_R as a function of percentage change in v_L and v_S, respectively.

Fig. 5. Changes in reflected profile (upper curves) due to three stepwise changes in v_S (lower curves).

of about 1.5% in the value of v_S can produce substantial changes in the reflected beam profile as the higher section shifts to the left while the intensity minimum becomes less pronounced. These results indicate that the shear wave velocity of the solid medium has a dominant influence in determining the nonspecular features. This can be seen from Fig. 4, where the percentage changes in v_R are plotted as functions of percentage changes in v_L and v_S, demonstrating that v_R is strongly related to v_S but is almost independent of small changes in v_L.

It can therefore be established from the preceding results that, in applying Rayleigh-angle nonspecular reflectivity to elastic defect characterization, defects can be reasonably specified by the value of the shear velocity only. The simplest type of elastic defects can then be specified by setting, for example,

$$V_S = \begin{cases} 3.23 \text{ km/s} & -w_0 \leqslant x \leqslant 0 \\ 3.13 \text{ km/s} & \text{otherwise} \end{cases} \quad (8)$$

This stepwise defect, which is of half-beamwidth size and centered at $x = -w_0/2$, is schematically represented by the curve of a step function below the x axis in Fig. 5. As the beam impinges upon the surface area which contains such a defect, the nonspecularly reflected beam is expected to have a quite different profile. Figure 5 shows a sharp increase in intensity in the left section of the reflected beam, where the elastic defect is present. With $v_S = 3.23$ km/s, v_S changes by 3% as the peak intensity of the left section of the beam becomes four times stronger. However,
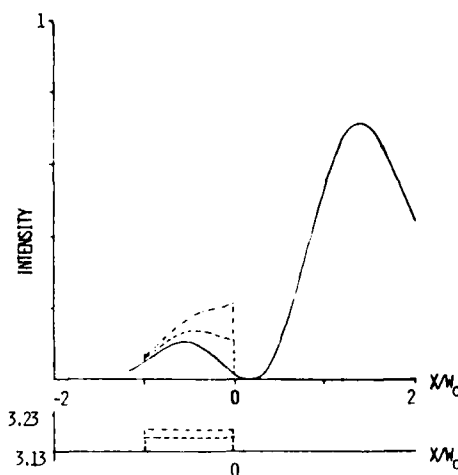
with a much smaller percentage change, 1% ($v_S = 3.17$ km/s), the change in the peak intensity of the left section is readily observable.

With elastic defects simply described by (8), the above results can serve to demonstrate the possibility of applying nonspecular effects of Rayleigh-angle reflection to defect characterization. Another specification of elastic defects, which is probably more realistic than that given by (8), can be achieved by
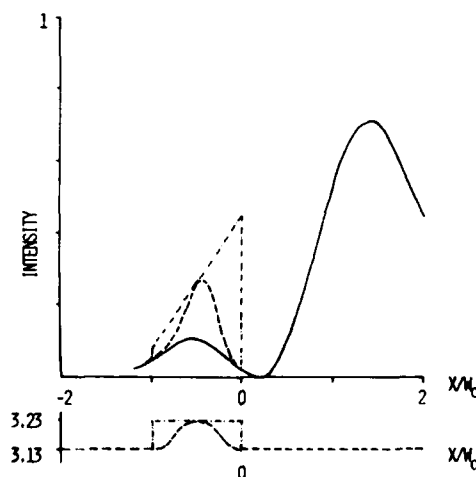

Fig. 6. Changes in reflected profile due to a smoothly varying elastic defect (upper curves). Variations of v_S are assumed to be sinusoidal (lower curves). Profile change shown in Fig. 5 is redrawn for comparison.

representing the shear velocity v_S in the form

$$V_S = \begin{cases} 3.18 + 0.05 \sin[2\pi(x + x_c)/s + \pi/2] \\ \quad \text{for} \quad x_c - s/2 \leqslant x \leqslant x_c + s/2 \\ 3.13 \quad \text{for} \quad x \geqslant x_c + s/2 \text{ and } x \leqslant x_c - s/2 \end{cases}$$

$$(9)$$

An elastic defect, as modeled by (9), has size s, and its center is located at $x = x_c$. A defect of type (9) is plotted in Fig. 6 along the x axis, where $s = w_0$ and $x_c = -w_0/2$. With this defect present, Fig. 6 shows the profile of a 2 MHz, 20 mm beam as it is reflected at the Rayleigh angle from the water-stainless steel interface. The left section of the beam is shown to be affected by the presence of the defect, having a much higher intensity. The resulting reflected profile now does not show any abrupt variation as shown in Fig. 5 when a stepwise defect is considered.

Fig. 7. Variation of defect characterizing profile as a function of defect location with defect centered (a) at $x/w_0 = -0.5$; (b) at $x/w_0 = 0$; (c) at $x/w_0 = +0.5$. Defect size and deviations as in Fig. 6.

4. DETERMINATION OF DEFECT SIZE AND LOCATION

The above calculations have illustrated how nonspecular reflectivity at the Raleigh angle can be utilized to detect an elastic defect. In other words, the nonspecularly reflected profiles are used as signatures that can determine whether such a defect exists. This application can be made more effective if information derivable from these signatures can point out where a defect is located, how large it is, and to what extent the elastic property deviates from the standard value. The following calculations are intended to illustrate how nonspecularly reflected profiles, when used as defect signatures, are sensitive to variations in defect size, location, and elastic deviation. In these calculations, the elastic defect under consideration is the smoothly varying type described by (9).

First, three reflected profiles were calculated for three locations of the elastic defect with its size being kept the same, $s = w_0$. The results are shown in Fig. 7 for $x_c = -w_0/2$, 0, and $w_0/2$. In Fig. 7, as the defect is moved from left to right, there appears an additional intensity peak that moves with it. Since the elastic defect causes the elastic property to deviate from that corresponding to Rayleigh-angle incidence, it is apparent that the part of the incident beam impinging upon the defect area undergoes a specular
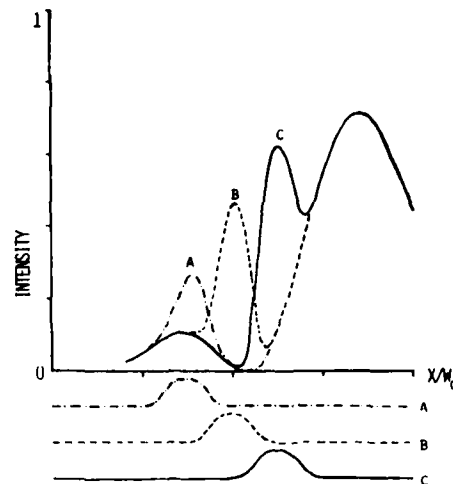
reflection. This specularly reflected beam section confirms the existence of the defect and also identifies where the defect is. In addition, the calculation results presented in Fig. 5 lead to the observation that the more the elastic defect deviates from the standard value, the stronger the intensity of the specular section is.
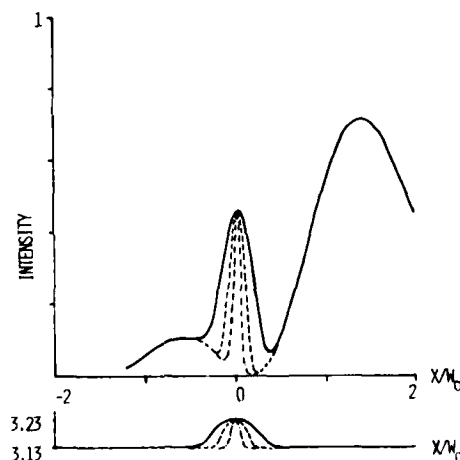

Fig. 8. Variation of defect characterizing profile as a function of defect size. Variation in defect size (lower curve) causes changes in beam profile (upper curve).

Next, the reflected profiles were calculated for different sizes of the elastic defect, $s = w_0$, $w_0/2$, and $w_0/4$. The location of the defect is determined by $x_c = 0$ and remains the same for all three calculations. The results are presented in Fig. 8 where the defect size is characterized along the position axis. It is established in this figure that the smaller the size of the defect becomes, the smaller the width of the specular beam section is. In other words, the size of the defect can be estimated by the width of the specular beam section.

5. CONCLUSIONS

In summary, the above calculation results have demonstrated that nonspecular reflectivity at the Rayleigh angle can be used to characterize a localized surface elastic defect. In this application, the non-specularly reflected profile serves as a signature of the elastic defect, whose size, location, and deviation of the shear velocity can be estimated by the width, position and intensity level of the specular beam section associated with the defect.

ACKNOWLEDGMENT

REFERENCES

1. H. L. Bertoni and T. Tamir, Unified theory of Rayleigh-angle phenomena for acoustic beams at liquid-solid interface, *Appl. Phys.* 2:157 (1973).
2. T. D. K. Ngoc and W. G. Mayer, Numerical integration methods for reflected beam profiles near Rayleigh angle, *J. Acoust. Soc. Am.* 67:1149 (1980).
3. T. D. K. Ngoc and W. G. Mayer, Ultrasonic nonspecular reflectivity near longitudinal critical angle, *J. Appl. Phys.* 50:7948 (1979).
4. T. D. K. Ngoc and W. G. Mayer, A general description of ultrasonic nonspecular reflection and transmission effects for layered media, *IEEE Trans. Sonics Ultrasonics* SU-27:229 (1980).
5. T. D. K. Ngoc and W. G. Mayer, Influence of plate mode structure and Gaussian beam profile characteristics on ultrasonic reflection and transmission, *IEEE Trans. Sonics Ultrasonics* SU-29:112 (1982).
6. W. G. Mayer, Detection of local inhomogeneities in solids by Rayleigh angle reflection, *Ultrasonics* 19:109 (1981).
7. W. G. Mayer and T. D. K. Ngoc, Acoustio-optic methods to locate surface inhomogeneities on solids, *J. Acoust. Soc. Am.* 70:S46 (1981).
8. D. E. Chimenti and L. Adler, Interaction of reradiated Rayleigh waves with fatigue cracks, *Ultrasonics* 19:112 (1981).
9. L. Brekhovskikh, *Waves in Layered Media* (Academic Press, New York, 1960).

Measurements of harmonic profiles of a bounded ultrasonic beam in a liquid medium

D.D. MCLENNAN, T.D.K. NGOC and W.G. MAYER

The acoustic field of a bounded finite-amplitude beam is governed by competing mechanisms such as medium non-linearity, interference, and attenuation. An analytic determination of the distribution of sonic energy in the individual harmonic components is often not reliable; consequently an experimental mapping of those harmonic components may be more appropriate. An experimental method is presented here which involves a miniature hydrophone probe which has been frequency calibrated for each harmonic component using a light diffraction technique. Measurements (made across the sound field) of the acoustic amplitude of the first three harmonic components are presented.

KEYWORDS: ultrasonics, transducer calibration, hydrophones

Introduction

Acoustic wave propagation is an inherently non-linear process. As a consequence of this non-linearity, an originally sinusoidal waveform distorts toward a sawtooth shape as it travels through a medium. Examination of the spectral content of the distorted waveform reveals that this distortion corresponds to the self-generation of harmonics within the sound beam. Thus, the harmonic content represents a quantitative measure of the waveform distortion.

Many ultrasonic experiments are conducted under conditions conducive to the production of significant wave distortion (that is, some combination of high initial intensity and long pathlengths). Moreover, numerous evaluation techniques using ultrasonics are based on the assumption that the probing beam contains only one frequency. If, however, sonic distortions are present, beam reflectivity, absorption, intensity distribution within the beam and other parameters may change sufficiently so that the evaluation of the received beam may lead to erroneous results if one does not take account of the multiple frequency components present in the originally sinusoidal beam.

Rather than attempting to determine analytically the distribution of ultrasonic energy as well as the degree of distortion present in all areas of the sound field, an often easier and more reliable method is to probe this sound field with a measuring device sensitive to the harmonic constituents.

Measurements of the harmonic distribution in an acoustic beam have been made[1,2] showing the profiles of the fundamental and some harmonics at several propagation distances.

The authors are in the Physics Department, Georgetown University, Washington DC 20057, USA. Paper received 15 January 1982. Revised 11 June 1982.

But, to obtain quantitative comparisons between the frequency-content distribution of the sound fields at different locations, it is necessary to make measurements with a probe whose frequency response is accurately calibrated.

In this paper, experimental investigation of non-linear harmonic generation involves quantitative measurements of the sound field of a low-MHz ultrasonic beam propagating in water using a calibrated miniature hydrophone.

Measurements were made in a region of the sound field that was useful experimentally, as well as in an area where all competing effects such as non-linearity, attenuation, and interference are significant. In the following, the experimental procedure is described in detail and the measured profiles of the first three harmonics are presented.

Experimental procedure

The experimental procedure is centred around two techniques:

(1) Mapping of the sound field by an electro-mechanical probe.

(2) Acousto-optic interaction for calibrating the probe.

The experimental set-up is therefore designed to accommodate both techniques. Because the calibration procedure is rather involved, it will be described separately.

Experimental methodology

Of the known methods currently in use,[3] the two techniques most often mentioned for mapping bounded acoustic beams are miniature hydrophones and diffraction of light by sound. The miniature hydrophone is suited for probing a small area, but it does not have a linear frequency response.[4] On the other hand, the light intensity of a diffraction order is independent of frequency but represents an integration

of the acoustic field across the sound beam. The experimental technique used here, employing a miniature hydrophone to map the sound field and a light diffraction set-up to calibrate the hydrophone, makes use of the major strengths of these two techniques.

The specific experimental set-up is illustrated in Fig. 1. The sound beam is generated along the z-axis and the translation of the probe is along the x-axis, across the sound beam. The electrical signal from the probe, representing the local sound field, is connected to a spectral analyser to select the desired harmonic component. The sound absorber is installed behind the probe to ensure that the ultrasonic beam consists of progressive waves only. The light diffraction system is also presented in Fig. 1. The combination of light source, lenses, and aperture produces a collimated light beam passing perpendicularly to the sound beam and forms a diffraction pattern on the face of the photodiode. The lenses and aperture were adjusted so as to maximize the spatial separation of the diffraction orders.

The source of the ultrasonic field was an air-backed quartz transducer driven at 3 MHz and having an effective radiating diameter of 2.0 cm. The probe used was a miniature hydrophone manufactured by Mediscan Incorporated with a circular detecting area 1.0 mm in diameter embedded in a hypodermic needle 1.3 mm in diameter. The detecting area of the probe is thus comparable to the sound wavelength and would therefore represent only a minimal disturbance to the sound field. In addition, the probe was inserted through a piece of sound absorbing rubber positioned in front of the electrical connection of the probe, thus eliminating the possibility of establishing a significant standing-wave pattern between transducer and probe.

Calibration

The measuring probe was calibrated using the diffraction of light by sound. The interaction of light with high-frequency sound manifests itself in the form of a diffraction pattern with the light intensity of the nth order being given by[5]

$$I_n = J_n^2(v) \tag{1}$$

where $J_n(v)$ is the nth-ordered Bessel function of the first kind. The argument v, the Raman-Nath parameter, of the above Bessel function is defined as

$$v = k p_0 L \, (\partial \mu / \partial p)_S \tag{2}$$
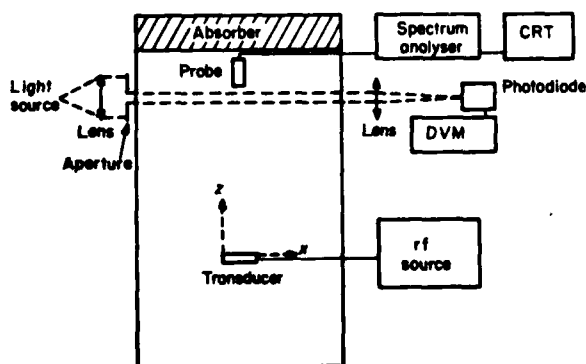

Fig. 1 Schematic of the experimental set-up. The sound beam travels in the z direction and the light beam in the x direction
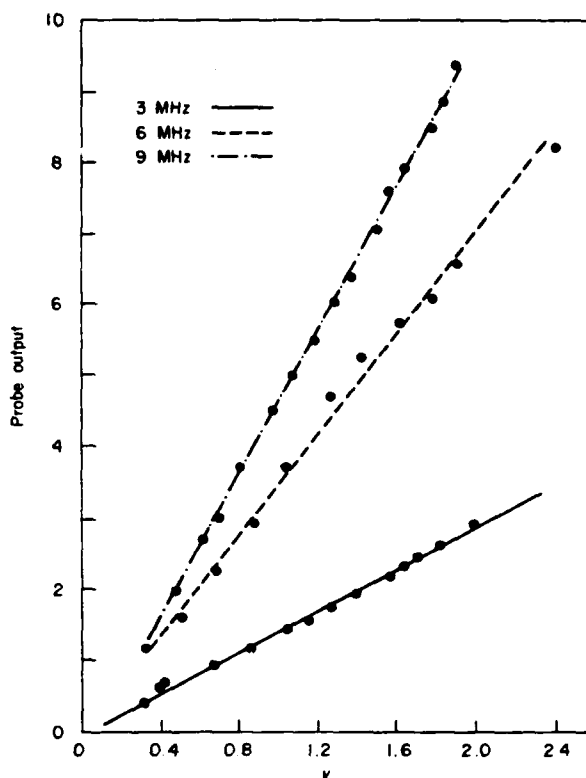

Fig. 2 Plot of Raman-Nath parameter against probe output for 3, 6, and 9 MHz. The parameter v is dimensionless and the sound amplitude is expressed in arbitrary units

where k is the wavenumber of light, p_0 the maximum acoustic pressure, L the interaction length, and $(\partial \mu / \partial p)_S$ the partial derivative of the refractive index with respect to pressure in adiabatic conditions. This partial derivative is identified as the piezo-optic coefficient. When a bounded sound beam is considered, the value of p_0 in (2) must be replaced by the maximum acoustic pressure averaged over the interaction length.

Within the narrow frequency range under consideration, the piezo-optic coefficient, and hence the Raman-Nath parameter, is independent of sound frequency.[6] As a result, (2) implies that there exists a linear relationship between the Raman-Nath parameter v and the acoustic pressure p_0, which is a measure of sound amplitude. In turn, v can be determined from the measured light intensity using (1).

The output of the measuring probe, which is considered to consist of the miniature hydrophone and the spectrum analyser, is calibrated against v derived from the known behaviour of $J_0^2(v)$ by measuring the percentage light intensity of the zeroth order. With reference to Fig. 1, the calibration was carried out with the light beam intercepting the sound field between the transducer and the hydrophone, which was positioned about 5 mm from the transducer face. In this manner, the diffracted light intensity and the probe output were simultaneously measured at different transducer driving voltages for 3, 6, and 9 MHz.

The values of v were derived following the above procedure and were then plotted against the probe output as illustrated in Fig. 2. It can be seen that the relationship between v and the probe output is linear for all frequencies. The slopes of

the three lines in Fig. 2, then, represent the specific response of the measuring probe to each frequency. Relative to the fundamental frequency, this response can be quantitatively described in terms of the ratios 1.0:2.9:3.5 for 3, 6, and 9 MHz, respectively.

Measurement of harmonic profiles

The above procedure was used to measure the local sound field as the sound waves travelled in water. Throughout the experiment the launched intensity was kept the same by setting the sound amplitude at the beam centre to correspond to $v = 2.4$, which is the first zero of $J_0^2(v)$, describing the light intensity of the zeroth order. This was also used as a procedure to check whether standing waves existed in the sound field, because the light intensity of the zeroth order[7] would not behave like $J_0^2(v)$ and would not go to zero at $v = 2.4$ in the presence of standing waves. In this experiment, the absence of significant standing waves was continually confirmed by this procedure.

Measurements were made across the sound beam at six different probe-to-source distances for 3, 6, and 9 MHz. Fig. 1 indicates that the position of the probe across the beam is described by the x-axis and the probe-to-source distance by the z-axis. As a result, three sets of beam profiles were obtained describing the variation of beam profiles as a function of probe-to-source distance under the influence of competing mechanisms: non-linearity, attenuation, and interference. These are presented in Figs 3–6.

Figure 3 shows typical beam profiles of three harmonic components measured at the same distance, $z = 21$ cm. The vertical scale, in arbitrary units, represents the measured sound amplitude, which has been adjusted in accordance with the calibration results obtained earlier. The lines connecting the points are meant to be a visual aid and do not represent a fit to the data.
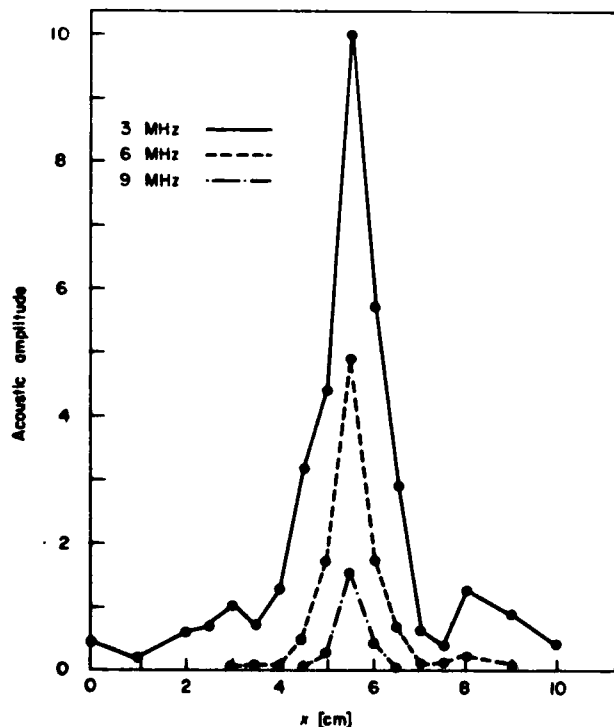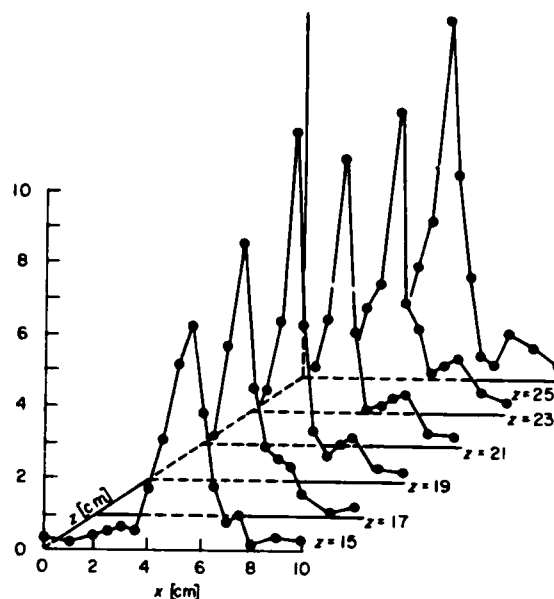

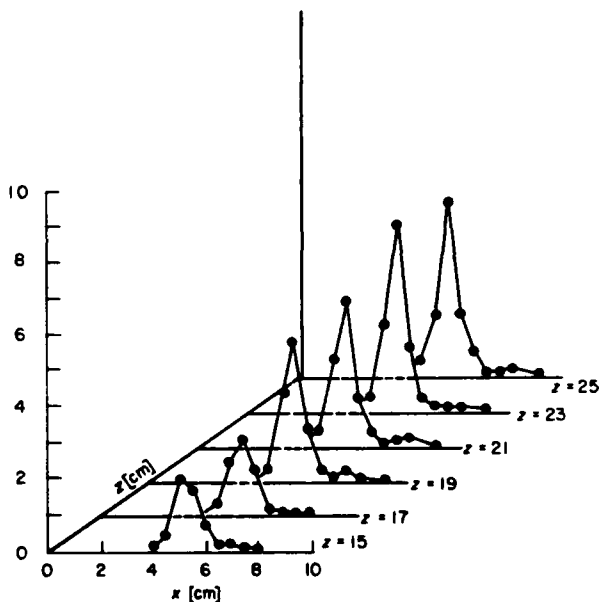Fig. 4   Variation of beam profile along the z direction for the fundamental frequency component

Fig. 5   Variation of beam profile along the z direction for the 6 MHz component

Figures 4–6 present the variation of beam profiles of 3, 6, and 9 MHz components along the z-axis. The values of probe-to-source distance range from 15 cm to 25 cm in 2 cm increments. These probe-to-source distances were chosen for investigation in order to have measurements made in a range where effects due to non-linearity, attenuation, and interference were believed to be significant while all harmonic components of interest were still measurable.

Some salient features of the beam profiles can be observed in Figs 4–6. The oscillatory variation in the maximum amplitude of the 3 MHz profiles shown in Fig. 4 points to the dominance of the interference process in determining the general profile shape. In Figs 5 and 6, the presence of the medium non-linearity mechanism is clearly seen in the steady growth of the 6 and 9 MHz profiles. Particularly in

Fig. 3   Representative profiles of the first three harmonics at $z = 21$ cm

Fig. 5, at z = 23 and 25 cm, the growth of the 6 MHz beam profiles seems to be levelling off, indicating a possible balance between the damping effect of attenuation and the growth of the harmonic due to medium non-linearity. For the near-Gaussian initial profile produced by the 3 MHz transducer under investigation, it is observed, in general, that the profiles of all harmonic components do not show any appreciable beam-spreading effect.

Conclusion

The above results establish that the employed experimental method, which combines miniature hydrophone measurement and a light diffraction technique, allows for a quantitative comparison of different harmonic components of a finite-amplitude bounded acoustic beam travelling in a liquid medium. From these results one can draw conclusions about the actual frequency-content of an ultrasonic beam which has travelled in a liquid medium before it is used to evaluate the properties of a sample to be tested. This knowledge appears to be important in all cases where the evaluation technique is frequency dependent.

Fig. 6 Variation of beam profile along the z direction for the 9 MHz component

References

1 Moffett, M.B. Measurement of Fundamental and Second Harmonic Pressures in the Field of a Circular Piston Source, *J. Phys.* (Paris) C8 (1979) 39

2 Gould, R.K., Smith, C.W., Williams, A.O. Jr., Ryan, R.P. Measured Structure of Harmonics Self Generated in an Acoustic Beam, *J. Acoust. Soc. Am.* 40 (1966) 421

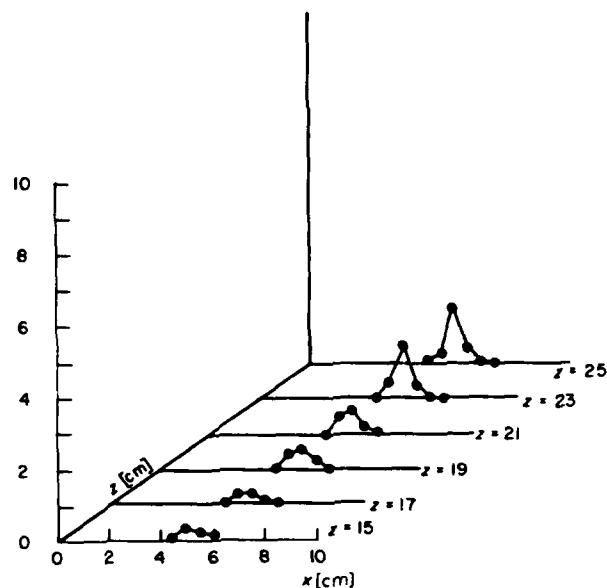3 Haran, M.E. Visualization and Measurement of Ultrasonic Wavefronts, *Proc. IEEE*, 67 (1979) 454

4 Harris, G.R., Herman, B.A., Haran, M.E., Smith, S.W. Calibration and Use of Miniature Ultrasonic Hydrophones, Proc. Biological Effects and Characteristics of Ultrasound Sources, (H.E.W.) 8048, (1978) 169

5 Raman, C.V., Nath, N.S. The Diffraction of Light by High Frequency Sound Waves: Part I, *Proc. Indian Acad. Sci.* 2A (1935) 406

6 Riley, W.A., Klein, W.R. Piezooptic Coefficients of Liquids, *J. Acoust. Soc. Am.* 42 (1967) 1258

7 Cook, B.D., Hiedemann, E.A. Diffraction of Light by Ultrasonic Waves of Various Standing Wave Ratios, *J. Acoust. Soc. Am.* 33 (1961) 945

MED

8